Lateralized Connectivity between Globus Pallidus and Motor Cortex is Associated with Freezing of Gait in Parkinson's Disease

Supplementary Methods

MRI data collection and processing

MRI Data collection. Imaging data was acquired using a 3 Tesla Siemens Magnetom Trio scanner with a 12-channel head coil at the Oregon Health and Science University's (OHSU) Advanced Imaging Research Centre. High-resolution structural 3D T1- and T2-weigthed images were obtained for co-registration with functional images. T1-weighted images were acquired using a sagittal magnetization prepared rapid gradient echo (MPRAGE) sequence (TR=2300 ms, TE=3.58ms, voxel size=1mm x 1mm x 1.1mm, slices=160). T2-weighted images were acquired using the following parameters: TR=3200 ms, TE=497ms, voxel size=1mm^3, slices=160). rs-fMRI BOLD images were obtained using a gradient-echo planar imaging (EPI) sequence (TR=2000ms, TE=30ms, field of view=240mm, flip angle=90°, voxel size=3.75x3.75x3.8mm). Steady-state magnetization was assumed after 5 frames (10s). Participants were instructed to relax but keep as still as possible with the eyes open while viewing a standard crosshair. All participants completed two rs-fMRI scans consisting of 10 minutes (300 frames) each to maximize the number of volumes that could be retained following data quality assurance. Only participants with at least 5 minutes of low head movement data (frame displacement less than 0.3 mm (Fair et al., 2013; Power et al., 2013, 2012) were included in the analysis.

MRI data preprocessing. Data were processed using surface-based registration (DCAN-Labs, 2019; Gilat et al., 2018; Glasser et al., 2013; Miranda-Dominguez et al., 2018) (available in github at https://github.com/DCAN-Labs/abcd-hcp-pipeline). This implementation includes the use of FSL (Jenkinson et al., 2012; Smith et al., 2004; Woolrich et al., 2009), FreeSurfer (Dale et al., 1999; Desikan et al., 2006; Fischl and Dale, 2000) and ANTs (Avants et al., 2011).

Briefly, T1-weighted and T2-weighted volumes are denoised first using DenoiseImage from ANTs (Manjón et al., 2010). Resulting images are linearly registered to the MNI's AC-PC axis and then non-linearly normalized to the MNI atlas using ANTs (Avants et al., 2011). Since ANTs' warps were not in the FSL readable format, they were converted to FSL format using c4d tool. This original alignment is refined using boundary-based registration (Greve and Fischl, 2009). Then, optimally aligned T1-weighted images are segmented using recon-all from FreeSurfer. Segmentations are improved by using the enhanced white matter-pial surface contrast of the T2-weighted sequence. Resulting segmentations are reported in native space (i.e., subject-specific) at a spatial density of 0.9 mm intervertex distance. Such values are downsampled and reported at a spatial resolution that has an intervertex spacing of 2 mm. This space is termed "the standard grayordinate space" and has of 91,282 anchor points (grayordinates) in the gray matter (surface and subcortical ROIs) (Glasser et al., 2013).

For resting state data, after slice time correction, the BOLD data is corrected for field distortions and registered preliminary to the first frame using a 6 degrees of freedom linear registration. After this initial alignment, the average frame is calculated and used as final reference. Next, the BOLD data is registered to this final reference and to the T1-weighted volume, all in one single step, by concatenating all the individual registrations into a single transformation matrix.

Surface-based registration. EPI data is registered, processed and reported at each grayordinate. To do this, the cortical ribbon obtained from the T1-weighted and T2-weighted volumes is used to define a mask. This mask is applied to the BOLD data to determine which voxels should be included and averaged together to calculate time series only from the gray matter. Voxels with partial coverage are also included via a weighted average. Weights reflects the percentage of volume contained within the ribbon. Calculation of weights is possible because the cortical ribbon has a higher spatial resolution than the BOLD data. In addition, voxels with high coefficients of variation, indicating poor tissue alignment or presence of large blood vessels, were excluded. The resulting time series from the cortical mesh are then down sampled into the standard grayordinate space. Time series are slightly smoothed in space using a 2-mm full-width-half-maximum Gaussian smoothing. The subcortical regions are registered as volumes but processed similarly (see (Glasser et al., 2013) for details). All the time series are reported in standard grayordinate space.

References

Avants, B.B., Tustison, N.J., Song, G., Cook, P.A., Klein, A., Gee, J.C., 2011. A reproducible evaluation of ANTs similarity metric performance in brain image registration. Neuroimage 54, 2033–44. https://doi.org/10.1016/j.neuroimage.2010.09.025

Dale, A.M., Fischl, B., Sereno, M.I., 1999. Cortical surface-based analysis. I. Segmentation and surface reconstruction. Neuroimage 9, 179–194. https://doi.org/10.1006/nimg.1998.0395

DCAN-Labs, 2019. DCAN-Labs/abcd-hcp-pipeline: v0.0.1: Singularity hotfix [WWW Document]. zenodo. URL https://zenodo.org/record/2605698#.XPAieBZKhph

Desikan, R.S., Segonne, F., Fischl, B., Quinn, B.T., Dickerson, B.C., Blacker, D., Buckner, R.L., Dale, A.M., Maguire, R.P., Hyman, B.T., Albert, M.S., Killiany, R.J., 2006. An automated labeling system for subdividing the human cerebral cortex on MRI scans into gyral based regions of interest. Neuroimage 31, 968–980. https://doi.org/S1053-8119(06)00043-7 [pii]10.1016/j.neuroimage.2006.01.021

Fair, D.A., Nigg, J.T., Iyer, S., Bathula, D., Mills, K.L., Dosenbach, N.U.F., Schlaggar, B.L., Mennes, M., Gutman, D., Bangaru, S., Buitelaar, J.K., Dickstein, D.P., Di Martino, A., Kennedy, D.N., Kelly, C., Luna, B., Schweitzer, J.B., Velanova, K., Wang, Y.-F., Mostofsky, S., Castellanos, F.X., Milham, M.P., 2013. Distinct neural signatures detected for ADHD subtypes after controlling for micro-movements in resting state functional connectivity MRI data. Front. Syst. Neurosci. 6, 80. https://doi.org/10.3389/fnsys.2012.00080

Fischl, B., Dale, A.M., 2000. Measuring the thickness of the human cerebral cortex from magnetic resonance images. Proc Natl Acad Sci U S A 97, 11050–11055. https://doi.org/10.1073/pnas.200033797

Gilat, M., Ehgoetz Martens, K.A., Miranda-Domínguez, O., Arpan, I., Shine, J.M., Mancini, M., Fair, D.A., Lewis, S.J.G.G., Horak, F.B., 2018. Dysfunctional limbic circuitry underlying freezing of gait in Parkinson's disease. Neuroscience 374, 119–132. https://doi.org/10.1016/j.neuroscience.2018.01.044

Glasser, M.F., Sotiropoulos, S.N., Wilson, J.A., Coalson, T.S., Fischl, B., Andersson, J.L., Xu, J., Jbabdi, S., Webster, M., Polimeni, J.R., Van Essen, D.C., Jenkinson, M., 2013. The minimal preprocessing pipelines for the Human Connectome Project. Neuroimage 80, 105–24. https://doi.org/10.1016/j.neuroimage.2013.04.127

Greve, D.N., Fischl, B., 2009. Accurate and robust brain image alignment using boundary-based registration. Neuroimage 48, 63–72. https://doi.org/10.1016/j.neuroimage.2009.06.060

Jenkinson, M., Beckmann, C.F., Behrens, T.E.J., Woolrich, M.W., Smith, S.M., 2012. FSL. Neuroimage 62, 782–790. https://doi.org/10.1016/j.neuroimage.2011.09.015

Manjón, J. V, Coupé, P., Martí-Bonmatí, L., Collins, D.L., Robles, M., 2010. Adaptive non-local means denoising of MR images with spatially varying noise levels. J. Magn. Reson. Imaging 31, 192–203. https://doi.org/10.1002/jmri.22003

Miranda-Dominguez, O., Feczko, E., Grayson, D.S., Walum, H., Nigg, J.T., Fair, D.A., 2018. Heritability of the human connectome: A connectotyping study. Netw. Neurosci. (Cambridge, Mass.) 2, 175–199. https://doi.org/10.1162/netn_a_00029

Power, J., Mitra, A., Laumann, T., Snyder, A., Schlaggar, B., Petersen, S., 2013. Methods to detect, characterize, and remove motion artifact in resting state fMRI. Neuroimage. https://doi.org/10.1016/j.neuroimage.2013.08.048

Power, J.D., Barnes, K.A., Snyder, A.Z., Schlaggar, B.L., Petersen, S.E., 2012. Spurious but systematic correlations in functional connectivity MRI networks arise from subject motion. Neuroimage 59, 2142–2154. https://doi.org/10.1016/j.neuroimage.2011.10.018

Smith, S.M., Jenkinson, M., Woolrich, M.W., Beckmann, C.F., Behrens, T.E.J.J., Johansen-Berg, H., Bannister, P.R., De Luca, M., Drobnjak, I., Flitney, D.E., Niazy, R.K., Saunders, J., Vickers, J., Zhang, Y., De Stefano, N., Brady, J.M., Matthews, P.M., 2004. Advances in functional and structural MR image analysis and implementation as FSL. Neuroimage 23, S208--19. https://doi.org/10.1016/j.neuroimage.2004.07.051

Woolrich, M.W., Jbabdi, S., Patenaude, B., Chappell, M., Makni, S., Behrens, T., Beckmann, C., Jenkinson, M., Smith, S.M., 2009. Bayesian analysis of neuroimaging data in FSL. Neuroimage 45, S173--86. https://doi.org/10.1016/j.neuroimage.2008.10.055

Figure S1. Connections with significant differences among the freezers (Ct), nonfreezers (PD-FoG) and control (Ct) groups at different motion censoring cutoffs and using matched and unmatched data. Distribution of the mean functional connectivity values for each ROI pair shown in Figure 2, color-coded *per* diagnosis (Ct, PD+FoG, PD-FoG). Circles represent the mean functional connectivity and the bar indicates the interquartile range. Thin lines correspond to the percentiles 2.5-97.5. As indicated on corresponding tables, each row corresponds to different conditions and different sample size: **A**. Frame displacement threshold of 0.3 mm, unmatched participants. **B**. Frame displacement threshold of 0.5 mm, matched participants. **C**. Frame displacement threshold of 0.5 mm, unmatched participants.

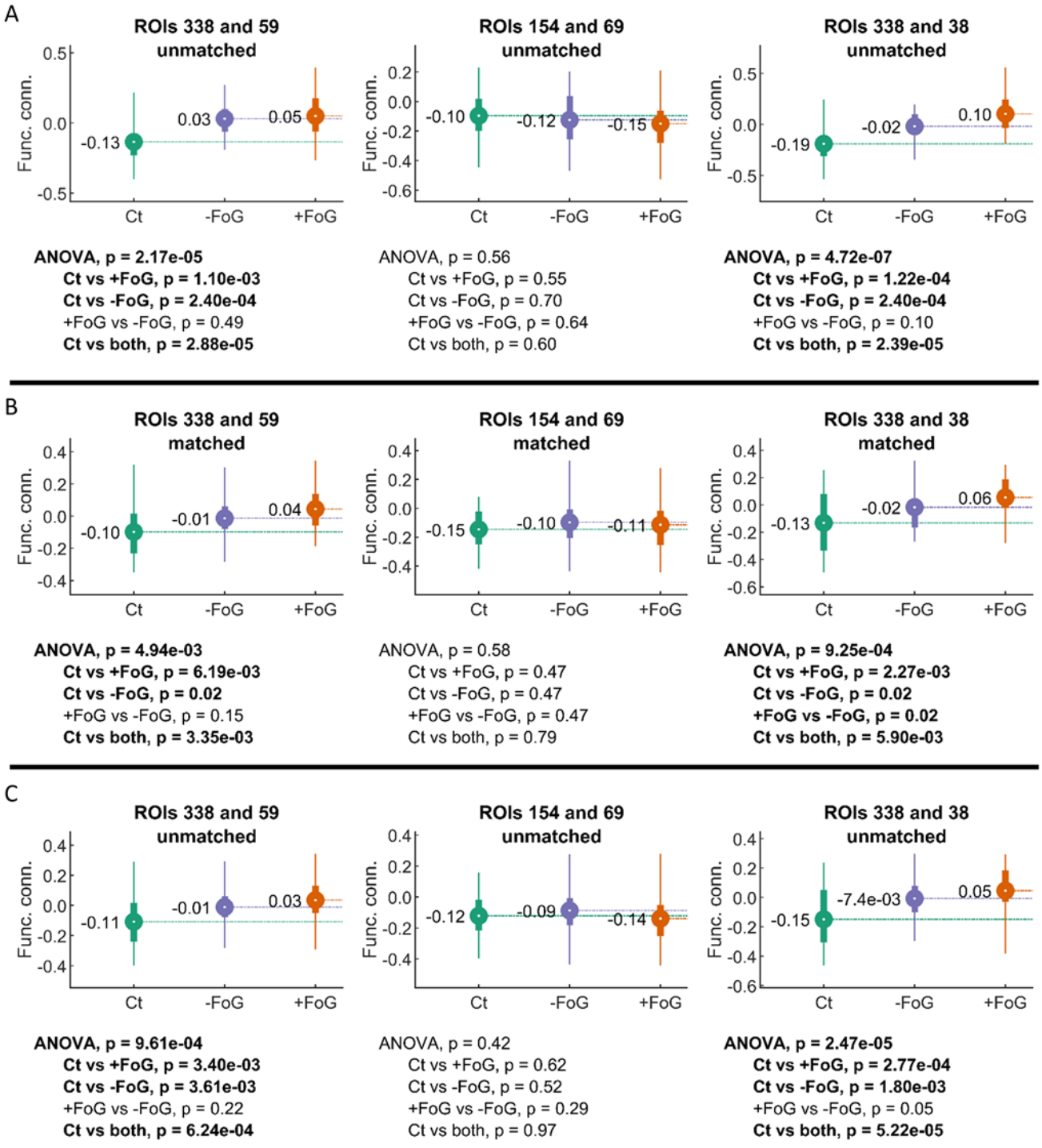

Supplementary Tables

Table S1. *p* -values from statistical comparisons among controls, PD freeers and PD non-freezers

Measurement	ANOVA	Kolmogorov-Smirnov test			
		Ct vs PD-FoG	Ct vs PD+FoG	PD-FoG vs PD+FoG	Ct vs both
Stride Length	**3.17E-05**	**0.008**	**1.44E-04**	0.151	**1.08E-04**
Pitch Angle at heel strike	**4.64E-05**	**2.48E-03**	**9.81E-04**	**0.028**	**2.05E-04**
Turning Average Peak Speed	**4.31E-04**	**3.49E-03**	**1.83E-03**	0.210	**9.05E-04**
Turning Average Jerk	**5.64E-04**	0.190	**2.48E-03**	**0.022**	**0.007**
Turning Average Duration	**6.09E-04**	**0.035**	**2.30E-04**	0.062	**1.22E-03**
Gait Speed	**3.97E-03**	0.071	**0.016**	0.303	**0.016**
FoG Ratio	**4.47E-03**	**0.047**	**8.81E-04**	**0.024**	**2.18E-03**
Dual task cost Gait Speed	0.700	0.424	0.184	0.210	0.341

Ct: Control participants. **PD-FoG**: Participants with Parkinson's disease without freezing of gait. **PD+FoG**: Participants with Parkinson's disease and freezing of gait. **Both**: PD-FoG and PD+FoG combined. **Numbers in bold text** are used to highlight comparisons with p -values < 0.05. **Text in bold** is used to highlight scores where all the paired comparisons were significant. Values sorted by decreasing p -value for the ANOVA test.

Table S2. Repeated measures ANOVA for effects of diagnosis, connectivity, networks and their interactions

Effect	Sum of squares	Degrees of freedom	Mean squares	F	p-value
Diagnosis	116.6	2	58.3	32.7	**<1e-6**
Individual connections	38363.0	46359	0.8	19.7	**<<1e-6**
Networks	16070.0	90	178.6	108.5	**<<1e-6**
Diagnosis and Connection	5767.6	92718	0.1	1.5	**0.008**
Diagnosis and Networks	1189.1	180	6.6	4.0	**<1e-6**

Table S3.Posthoc comparisons per functional networks

Networks	ANOVA p-value (corrected)	post-hoc p-values		
		Ct vs PD+FoG	Ct vs PD-FoG	PD+FoG vs PD-FoG
Sml and Sml	<0.001	<0.001	<0.001	0.412
Def and SMm	<0.001	<0.001	<0.001	0.929
SMm and Sml	0.001	<0.001	<0.001	0.815
Sml and Sub	0.003	<0.001	0.010	0.249
SMm and Sub	0.003	<0.001	0.002	0.761
CiO and Def	0.006	0.003	<0.001	0.937
Def and DoA	0.012	0.005	0.002	0.986
Def and Sub	0.014	<0.001	0.068	0.236
DoA and Vis	0.029	0.002	0.318	**0.088**

Sml, Somatosensory lateral; Def, Default; SMm, Somatosensory medial; CiO, Cingulo-Opercular; DoA, Dorsal Attention; Sub, subcortical; Vis, visual

Table S4. Connection pairs with significant difference between diagnostic groups.

Pair of ROIs	Corrected p-values		
	Ct vs PD+FoG	Ct vs PD-FoG	PD+FoG vs PD-FoG
I. Left motor (Gordon 59) and left globus pallidus	7.80E-06	0.025	0.026
II. Left vestibular (Gordon 69) and left default (Gordon 154)	8.09E-06	0.030	0.023
III. Left motor (Gordon 38) and left globus pallidus	1.21E-05	0.045	0.020